DESIGN OF A PITCH-ROLL JOYSTICK BASED ON A THREE-LOBE SPHERICAL CAM MECHANISM

Debal Saha, Jorge Angeles and Jozsef Kövecses
Department of Mechanical Engineering, McGill University, Montréal, Canada
E-mail: debalsaha@cim.mcgill.ca; jorge.angeles@mcgill.ca; jozsef.kovecses@mcgill.ca

Received July 2015, Accepted November 2015
No. 15-CSME-65, E.I.C. Accession 3840

ABSTRACT
A pitch-roll joystick based on a spherical cam mechanism is proposed that can be implemented as a haptics device. Spherical cams can replace the bevel gears that are conventionally used in transmission mechanisms involving shafts with intersecting axes to achieve lower backlash, lower frictional losses and higher stiffness. Such a spherical cam mechanism is essentially composed of multi-lobe-cams and conical rollers. Undercutting is a deterrent to the generation of smooth cam surfaces, which calls for the synthesis of a singularity-free spherical cam profile. The issues of high pressure angle and high contact ratio are addressed by means of a multilobe cam. The design of the cam profile and the assembly of the joystick are described. The criteria for the selection of the numbers of lobes and rollers are also explained.

Keywords: spherical multi-lobe cam; pitch-roll joystick; pressure angle.

LA CONCEPTION D'UN MANCHE À BALAI TANGAGE-ROULIS BASÉ SUR UN MÉCANISME À CAMES SPHÉRIQUES À TROIS LOBES

RÉSUMÉ
Un manche à balai tangage-roulis basé sur un mécanisme à cames sphériques est proposé. Ce dernier peut être conçu comme dispositif haptique. Les mécanismes à cames sphériques peuvent remplacer les engrenages coniques car ils offrent un jeu et des pertes plus faibles dues au frottement de ces derniers, tout en augmentant la rigidité de l'ensemble. Ces mécanismes sont essentiellement composés de cames multilobes et de roulements coniques. Pour éviter la contre-dépouille, il faut synthétiser un profil de came sphérique libre de singularités. Les cames à plusieurs lobes permettent de résoudre le problème posé par un angle de pression et un rapport de contact trop élevés. Les auteurs proposent un manche à balai tangage-roulis basé sur un mécanisme à cames de type sphérique qui puisse servir de dispositif haptique. Ils traitent de la conception du profil de la came, de l'assemblage du manche à balai et du choix du nombre de lobes et de lobes et de roulements.

Mots-clés : came sphérique multilobe; manche à balai tangage-roulis; angle de pression.

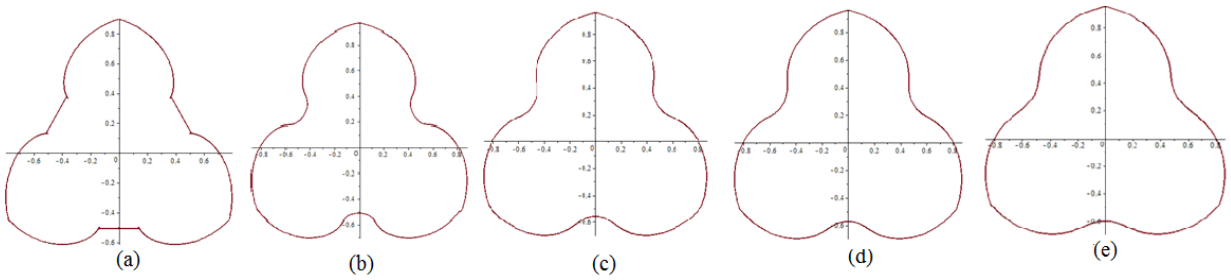

Fig. 1. Cam-profiles for three lobes: (a) one roller, (b) two rollers, (c) three rollers, (d) four rollers, (e) five rollers.

1. INTRODUCTION

The traditional means employed for motion and force transmission between two perpendicular shafts is bevel gears. These entail some inherent drawbacks, like high backlash and high friction, that render the use of bevel gears for applications in robotic wrists and haptics devices incapable of delivering the desired level of performance. Such applications require, first and foremost, low noise levels, while noise arises from dry friction, backlash and compliance, as present in gear transmissions. Spherical cam mechanisms provide suitable substitutes for bevel gears, as observed by Bai et al. [1]. A cam-follower mechanism is proposed here that is essentially composed of a spherical cam and a follower with conical rollers. The rollers and the cam provide favorable features to the cam mechanism, like high stiffness, high contact ratio, low friction and low backlash. Various other advantages that spatial cam mechanisms, in general, possess over gear transmissions are cited by Wei et al. [2].

A pitch-roll joystick based on a spherical cam mechanism is proposed that is intended for haptic applications. The design of the various parts of the joystick are conceptualized based on the recommendations found in the literature [3–6], while developing joysticks for various purposes. The number of lobes and rollers for the multi-lobe cam (MLC) are decided to be three and four, respectively, as opposed to four and seven for a previous mechanism [1], as this combination results in various advantages like design simplification, reduced manufacturing complexity and suitable values for cam-design parameters, such as radius of curvature and pressure angle. Plots of cam profiles with three lobes and number of rollers varying from one to five are shown in Fig. 1.

Certain issues need to be addressed while implementing spherical cam mechanisms as substitutes of bevel gears. The singularities in cam profile leading to undercutting, together with a variable pressure angle, are considered and resolved for better transmission in the proposed mechanism for the pitch-roll joystick. The transmission quality, dictated by the pressure-angle distribution, is also affected by the contact ratio; it is duly studied for the MLC case.

The assembly of the pitch-roll joystick implementing the cam-follower mechanism is then described, the mechanism performance assessed by kinematic simulation. Conclusions are then drawn for the suitability of the proposed joystick as a haptic device and other prospective applications.

2. GENERATION OF THE CAM-PROFILE

The geometric fundamentals that govern the design and operation of cam mechanisms are studied under the branch of kinematic synthesis; they can be categorized in a specific class called cam synthesis. The principles that govern the kinematics of spherical cam mechanisms are explained by describing the procedure for the generation of their ruled pitch surfaces.

The spherical curves required for cam-profile synthesis are generated by application of the *Aronhold–Kennedy Theorem* (AKT), which states that when three bodies are in relative motion, the three *Instant Screw*

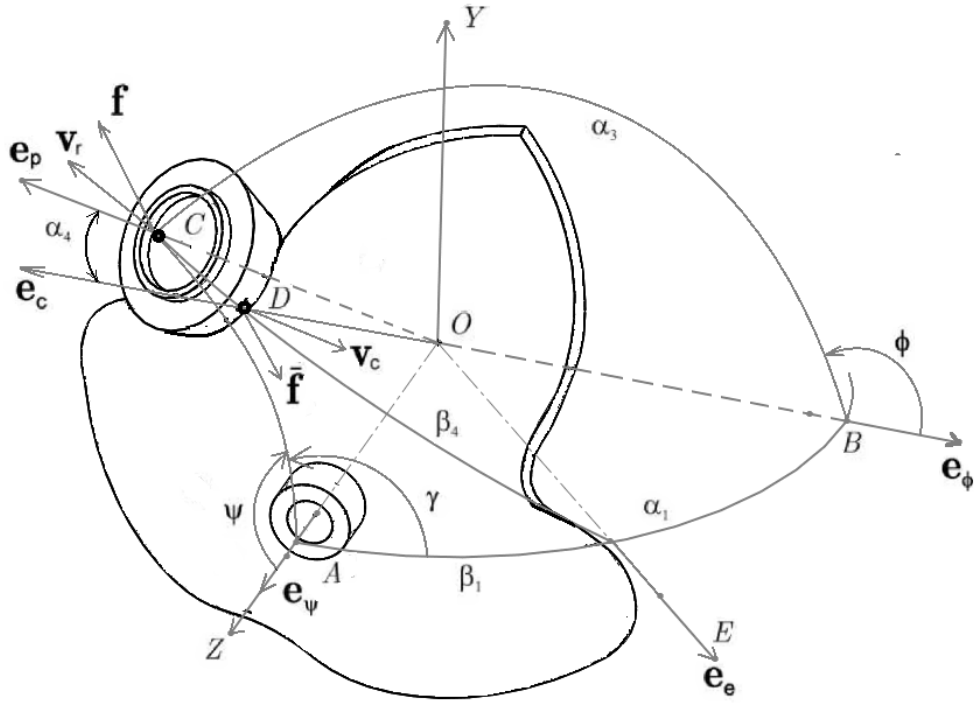

Fig. 2. Axes and angles defined for the spherical cam mechanism.

Table 1. Definition of unit vectors used for cam-profile synthesis.

Notation	Definitions
$\mathbf{e}_\psi$	Vector parallel to the axis of the cam rotation w.r.t. the frame
$\mathbf{e}_\mathrm{p}$	Vector parallel to the roller-shaft axis
$\mathbf{e}_\mathrm{e}$	Vector parallel to the instant axis of rotation of the cam w.r.t. the follower
$\mathbf{e}_\phi$	Vector parallel to the follower shaft
$\mathbf{e}_\mathrm{c}$	Vector parallel to the axis of rotation of the roller w.r.t. the cam

Axes (ISAs), associated with the three pairs of bodies under relative motion, have one common perpendicular [7]. In the case of spherical motion the ISA becomes *Instant Axis* (IA) of rotation, with all IAs intersecting at one common point, the centre of the spherical motion in question. In this case, the AKT states that all three IAs are coplanar. The ruled surfaces generated by the rotation of the IAs play a key role in the synthesis of the desired cam profile.

The proposed device is a four-link spherical mechanism comprising a spherical cam, a follower, a roller and a frame. To generate its cam profile, the IAs of the rotation of the links w.r.t. each other are first identified.

The nomenclature for the vectors and the angles useful for cam-profile generation is illustrated in Fig. 2. The design of interest is based on both ergonomics data drawn from the specialized literature [3–6] and the dimensions of off-the-shelf components, as discussed in Subsection 6.1. All the elements of a spherical cam mechanism are shown in Fig. 2.

The cam-profile is a conical surface with two spherical curves as its concentric boundaries, which are defined by the curves of intersection of the conical surface with two concentric spheres. The conical surface

Table 2. Angles used for cam-profile synthesis.

Notation	Definitions
α_1	Angle between the axis of the cam and that of the roller carrier ($\angle AOB$)
α_3	Angle subtended by the arc of the roller carrier ($\angle BOC$)
α_4	Half angle subtended by the conical roller ($\angle COD$)
β_1	Angle between the cam axis and the IA of the follower w.r.t. the cam ($\angle AOE$)
β_4	Angle between the axis of the roller and the IA of the follower w.r.t. the cam ($\angle COE$)

is generated by the spherical motion of the IA of rotation of the roller w.r.t. the cam. The position vector of an arbitrary point of these curves is given by an expression obtained by rotating a vector through the roller-cam contact point about the cam axis (parallel to the Z-axis of the reference frame).

M and N denote the number of lobes and rollers of the roller-carrier, respectively, as needed in developing the kinematic relations relevant to cam-profile generation and analysis of singularities and pressure-angle distribution. The angles of rotation of the cam and the roller-carrier are represented by ψ and ϕ, respectively. The input-output relation is given below:

$$\phi = -\frac{M}{N}\psi + \phi_0 \tag{1}$$

The initial position of the cam at $\psi = 0$, denoted by ϕ_0, is defined such that the crest of one of its lobes lies in the axis, say at $x = 0$, or the Y-axis. We thus have $\phi_0 = (1 - 1/N)\pi$.

The first step for cam-profile generation consists in defining the reference frame required to represent the rotations of the various links. The global reference frame is defined as one fixed to the frame of the mechanism, with the Z-axis defined as the axis of rotation of the cam w.r.t. the frame. Using the standard rotation matrices about X, Y and Z-axes [9] along with the angles subtended on the unit sphere shown in Fig. 2 and the nomenclature for the vectors along the axes of rotation, the relations below follow:

1. $\mathbf{e}_\psi = \mathbf{e}_\mathrm{z} = [0 \quad 0 \quad 1]^\mathrm{T}$
2. $\mathbf{e}_\mathrm{p} = \mathbf{Q}_\mathrm{y}(\alpha_1)\,\mathbf{Q}_\mathrm{z}(\phi)\,\mathbf{Q}_\mathrm{y}(\alpha_3)\mathbf{e}_\mathrm{z}$
3. $\mathbf{e}_\mathrm{e} = \mathbf{Q}_\mathrm{y}(\beta_1)\mathbf{e}_\mathrm{z}$
4. $\mathbf{e}_\phi = \mathbf{Q}_\mathrm{y}(\alpha_1)\mathbf{e}_\mathrm{z}$

First, angle β_4 is calculated:

$$\cos\beta_4 = \mathbf{e}_\mathrm{e}^\mathrm{T}\mathbf{e}_\mathrm{p} \tag{2}$$

Upon expansion of the right-hand side of Eq. (2), we obtain

$$\begin{aligned}\cos\beta_4 = {} & \sin\beta_1\cos\alpha_1\cos\phi_1\sin\alpha_3 + \sin\beta_1\sin\alpha_1\sin\alpha_3 \\ & - \cos\beta_1\sin\alpha_1\cos\phi\sin\alpha_3 + \cos\beta_1\cos\alpha_1\cos\alpha_3\end{aligned} \tag{3}$$

Further, γ is the angle of rotation of the conical roller about the instant axis of rotation OE, as shown in Fig. 2; it is given by

$$\cos\gamma = \csc(\alpha_1 - \beta_1)\csc\beta_4[\cos\alpha_3 - \cos(\alpha_1 - \beta_1)\cos\beta_4] \tag{4}$$

The position vector $\mathbf{s}_\mathrm{c}$ of a point on the spherical curve defining the profile is obtained by using vector $\mathbf{e}_\mathrm{c}$ and the rotation matrix $\mathbf{Q}_\mathrm{z}$ representing the rotation about the cam-axis through the angle, ψ of rotation of

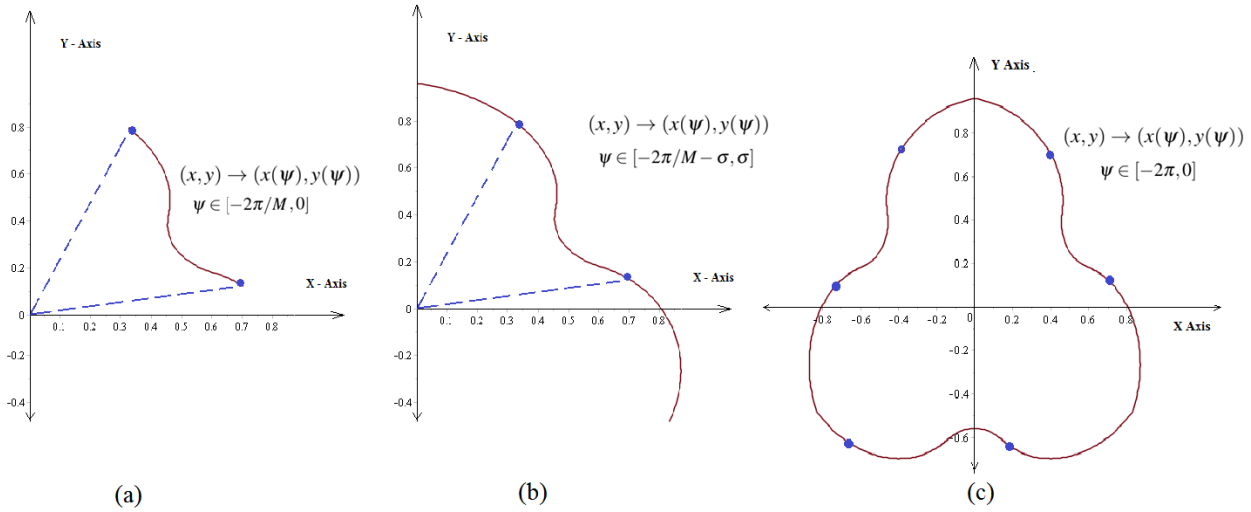

Fig. 3. (a) Complete pitch curve of the cam-profile when projected onto the X-Y plane; (b) complete cam-profile in two dimensions; (c) conical surface defining the spherical cam-profile intersecting the sphere on which the spherical mechanism is based.

the cam, i.e.,

$$\mathbf{s}_c = \mathbf{Q}_z^T(\psi)\mathbf{e}_c = \begin{bmatrix} c\phi s\gamma s\beta_3 - s\psi(c\beta_1 c\gamma s\beta_3 + s\beta_1 c\beta_3) \\ s\psi s\gamma s\beta_3 - c\psi(c\beta_1 c\gamma s\beta_3 + s\beta_1 c\beta_3) \\ s\beta_1 c\gamma s\beta_3 + c\beta_1 c\beta_3 \end{bmatrix} \tag{5}$$

where s stands for sine and c for cosine. With all the above relations simplified, the only variable of the position vector of the cam-profile is the input angle ψ of the cam. In other words, we have the vector for the cam-profile generation as a function of ψ, given as $\mathbf{s}_c = \mathbf{s}_c(\psi)$. The projection of the generated cam profile onto the X-Y plane is shown in Fig. 3(c).

Similarly, the spherical curve generated upon rotating vector $\mathbf{e}_p$ throughout the same rotation matrix for a rotation about the cam-axis, called the *pitch curve*, is given by

$$\mathbf{s}_p = \mathbf{Q}_z^T(\psi)\mathbf{e}_p = \begin{bmatrix} s\psi s\phi s\alpha_3 + c\psi(c\alpha_1 c\phi s\alpha_3 + s\alpha_1 c\alpha_3) \\ c\psi c\phi s\alpha_3 - s\psi(c\alpha_1 c\phi s\alpha_3 + s\alpha_1 c\alpha_3) \\ s\alpha_1 c\phi s\alpha_3 + c\alpha_1 c\alpha_3 \end{bmatrix} \tag{6}$$

The position vector of the pitch curve obtained above is used to derive an expression for the *radius of curvature* of the cam-profile.

The cams of the proposed spherical cam mechanism are designed with three lobes, i.e., $M = 3$. The curve generated by Eq. (5) is incomplete; it needs to be defined for an extended range of ψ, which requires finding an *extension angle* σ, that is obtained by solving the equation $\mathbf{s}_c(\psi)|_{\psi=\sigma} = \mathbf{0}$. The plot of the extended curve is obtained for $\psi \in [-2\pi/M - \sigma, \sigma]$, as shown in Fig. 3(b).

The extended curve is then rotated $M - 1 = 2$ times more, about the origin, through an angle of 120° to obtain the complete two-dimensional cam-profile, as shown in Fig. 3(c). Computer algebra is used to manipulate the relations between the various variables and parameters of the mechanism, from which the position vector of an arbitrary point of the pitch curve of the cam-profile is obtained. The spherical curve representing the cam-profile is shown in Fig. 4, obtained as the intersection of the conical surface of the cam with the sphere on which the spherical mechanism is based.

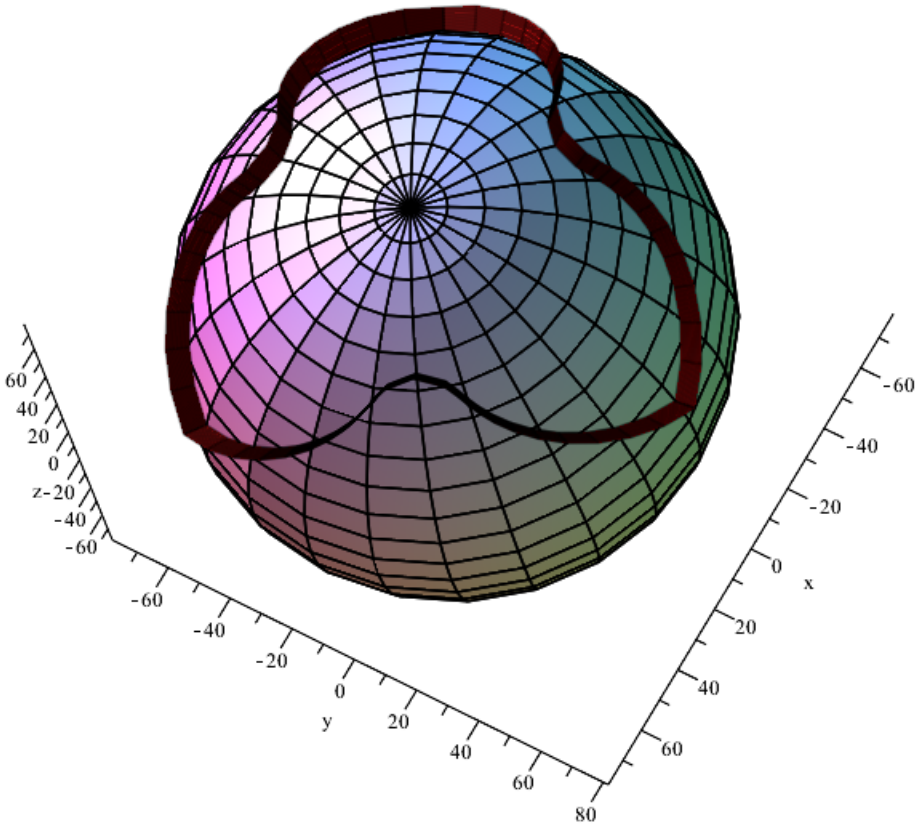

Fig. 4. The three dimensional plot of the conical surface that defines the spherical cam-profile intersecting the sphere on which the spherical mechanism is based.

3. SINGULARITIES AND UNDERCUTTING AVOIDANCE

The study of singularities is vital, as singularities are the vulnerable points where *undercutting* may occur. *Undercutting* is the recess at a point in an otherwise smooth profile where there is an abrupt change of curvature due to presence of singularities like double points or cusps. To avoid *undercutting*, a limiting value needs to be calculated for the *radius of curvature*, denoted by ρ. As explained by McCarthy and Roth [8], the *radius of curvature* is related to the position vector $\mathbf{s}_\mathrm{p}$ of the pitch curve by

$$\tan\rho = \frac{\| \mathbf{s}'_\mathrm{p} \|^3}{\mathbf{s}_\mathrm{p} \times \mathbf{s}'_\mathrm{p} \cdot \mathbf{s}''_\mathrm{p}} \tag{7}$$

In Eq. (7), the prime denotes the derivative with respect to the input angle ψ, the double prime the second derivative. *Undercutting* takes place at the minimum radius of curvature of the cam-profile, which can be obtained from the relation given in Eq. (7), upon equating the numerator to zero:

$$\frac{\partial \mathbf{s}_\mathrm{p}}{\partial \psi} = \mathbf{0} \tag{8}$$

The minimum radius of curvature occurs at the value of ψ where the roller axis lies closest to the cam axis. This value is $\psi = \pi/M$. Thus, Eq. (8) leads to

$$\tan\bar{\alpha}_3 = \frac{N}{M} \tag{9}$$

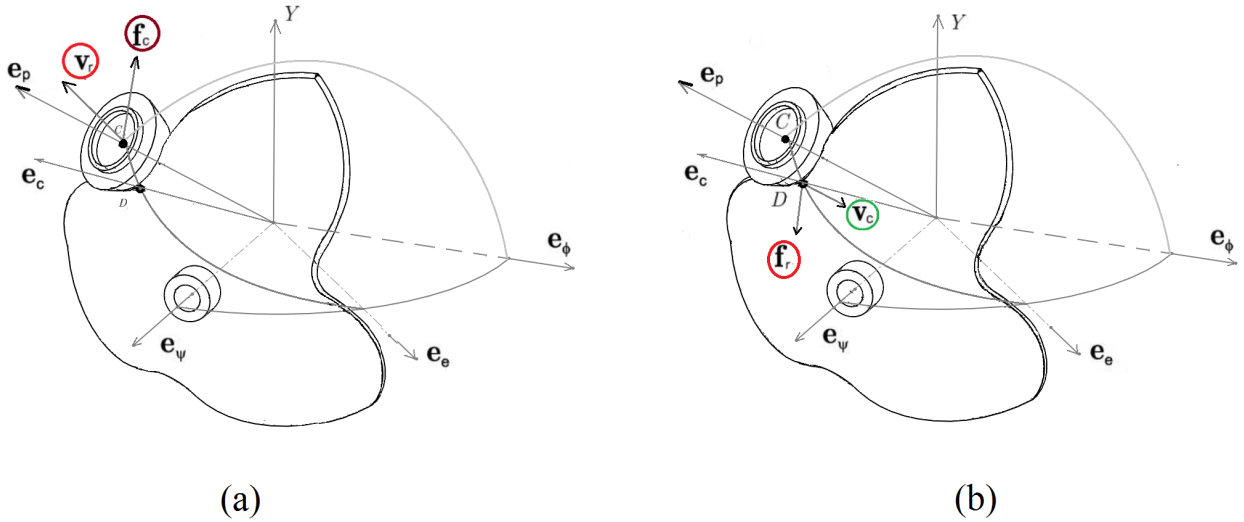

Fig. 5. Illustration of the pressure angle: (a) positive action; (b) negative action.

Here $\bar{\alpha}_3$ denotes the critical value of α_3, the angle subtended by the arc representing the roller carrier. This value just gives an upper bound for α_3 to avoid undercutting. The plots of the cam-profile are obtained for various values of α_3 ($< \bar{\alpha}_3$); the one with a smooth profile that ensures undercutting-avoidance is chosen.

4. PRESSURE ANGLE

The pressure angle of spherical cam mechanisms is that between the line of action of the force applied by the driving element and the direction of the velocity of the contact point of its driven counterpart. The positive and the negative actions of the cam mechanism are first described, then expressions for the pressure angle in both cases are obtained.

4.1. Reversible Action

The spherical cam mechanism considered in this report is reversible, which means that any of both cam and roller-carrier can play the role of the driving, the other of the driven element. The two types of action and the corresponding expression of the pressure angle are explained below.

4.1.1. Positive action

In this case the cam drives the roller-carrier. The driving force is $\mathbf{f}_c$, the pressure angle then being defined as that between the line-of-action of this force and the direction of the velocity vector $\mathbf{v}_r$ of the contact point on the driven roller-carrier. Both $\mathbf{f}_c$ and $\mathbf{v}_r$ are identical to those related to the centre of the roller, as shown in Fig. 5(a). The roller centre describes a curve offset w.r.t. the cam profile on the unit sphere, termed the *pitch curve*.

Here $\mathbf{f}_c$ is the unit vector along the force applied by the cam, while $\mathbf{v}_r$ is the velocity vector of the roller-carrier at the intersection of roller axis and unit sphere.

The relation for the pressure angle under positive action, denoted by μ_p is thus obtained as

$$\tan \mu_p = \frac{\| \mathbf{f}_c \times \mathbf{v}_r \|}{\mathbf{f}_c \cdot \mathbf{v}_r} \tag{10}$$

Notice that, in Eq. (10), the magnitudes of force $\mathbf{f}_c$ and velocity $\mathbf{v}_r$ are immaterial; what matters is only their directions. Henceforth, the magnitudes of these vectors are simply ignored; therefore, these vectors are

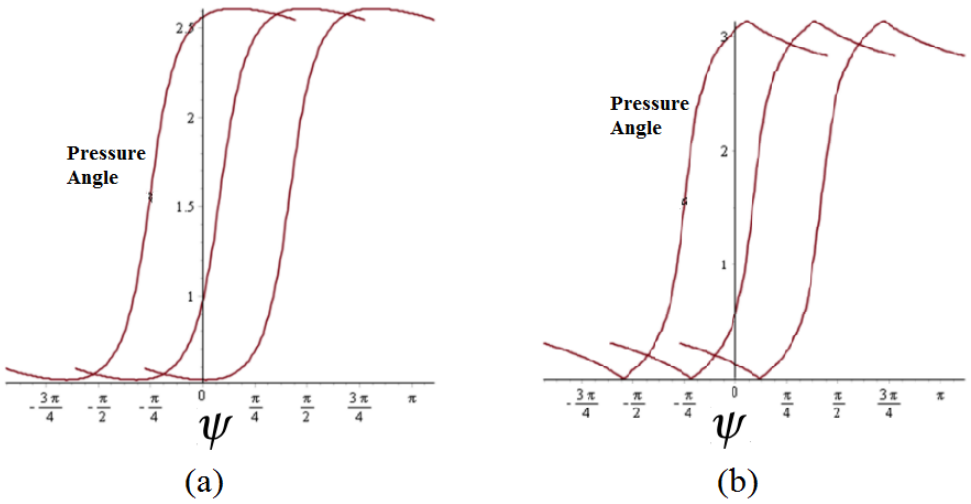

Fig. 6. Pressure angle for negative action with: (a) $M = 3$, $N = 4$, $\alpha_3 = \tan^{-1}(M/N) - 0.0174$; (b) $M = 3$, $N = 4$, $\alpha_3 = \tan^{-1}(M/N) - 0.0348$.

given by

$$\mathbf{f}_c = \mathbf{e}_p \times (\mathbf{e}_p \times \mathbf{e}_e) \tag{11}$$

$$\mathbf{v}_r = \mathbf{e}_p \times \mathbf{e}_\phi \tag{12}$$

4.1.2. Negative action

In this case the roller-carrier drives the cam. The direction of the force, given by vector $\mathbf{f}_r$, and that of the velocity vector, $\mathbf{v}_c$, are shown in Fig. 5(b).

The expression for the pressure angle, denoted by μ_n, is given below

$$\tan \mu_n = \frac{\| \ \mathbf{f}_r \times \mathbf{v}_c \ \|}{\mathbf{f}_r \cdot \mathbf{v}_c} \tag{13}$$

where, again the magnitudes of $\mathbf{f}_r$ and $\mathbf{v}_c$ are immaterial.

Here $\mathbf{f}_r$ is a vector parallel to the force applied by the roller-carrier, while $\mathbf{v}_c$ is the velocity of the cam at the intersection of the generatrix of the cam conical surface with the unit sphere. Expressions for these vectors are given as

$$\mathbf{f}_r = \mathbf{e}_c \times (\mathbf{e}_e \times \mathbf{e}_c) \tag{14}$$

$$\mathbf{v}_c = \mathbf{e}_\phi \times \mathbf{e}_c \tag{15}$$

4.2. Pressure Angle Plots

The *distribution* of the pressure angle depends on three parameters, M, N and α_3. From the singularity-analysis, the profile is found to have a smoother shape with an increase in the number of rollers. Negative action is implemented to drive the spherical cam mechanism. Pressure angle plots are obtained for negative action; it is found that the pressure angle grows with the number of rollers. Thus, the optimum number of rollers is chosen to be four. Typical plots for pressure-angle distribution are shown in Fig 6.

5. CONTACT RATIO

The contact ratio for cam mechanisms m_p is defined similar to gears, as the ratio of the action angle ψ_{a} to the pitch angle ψ_{p} as explained by Bai et al. [1]. If ψ_{a} is defined as the angle of rotation of the cam for which it is in contact with a single roller and for the pitch angle we have $\psi_{\mathrm{p}} = 2\pi/M$. Then

$$m_p = \frac{\psi_{\mathrm{a}}}{\psi_{\mathrm{p}}} = \frac{2\pi/M + 2\sigma}{2\pi/M} = 1 + \frac{M\sigma}{\pi} \tag{16}$$

A contact ratio greater than unity ensures continuous roller-cam contact and a pure rolling motion between roller and cam.

6. A PITCH-ROLL JOYSTICK

6.1. Design of the Joystick

The design of pitch-roll joystick reported here is based on the spherical cam mechanism synthesized above, with the layout of a differential mechanism, thereby offering two degree-of-freedom (d.o.f) motion. One d.o.f, the rolling, takes place about the axis of the roller carrier, the second, or pitching, about the cam axis.

The plots for various cam-profiles of a cam with three lobes are obtained for various values of number of rollers N and angle α_3, as illustrated in Fig 6. With an increase in the number of rollers, the profile is found to be smoother. Negative action is implemented to drive the spherical cam mechanism. Pressure angle plots are obtained for negative action; it is found that the pressure angle grows with the number of rollers, which is chosen as four. In cam design it is recommended to keep the pressure angle within 30° [10].

The joystick consists of two pairs of spherical cams placed in a diametrically opposed layout. Each pair has an inner, smaller cam and an outer, larger cam. These two cams form a set of coaxial conjugate cams that are keyed rigidly into a single cam shaft and positioned at a 60° phase angle. This means that the crest of a lobe of one of the cams lies at the trough of the lobe of the corresponding conjugate cam. The roller-carrier, rigidly attached to the handle to which it is keyed, provides two-d.o.f. motion capabilities. The carrier holds two sets of four rollers, one outer set and one inner set. The outer rollers engage with the outer cams, the inner rollers with the smaller, inner cams. The roller stands that carry the rollers are press-fitted on holes on the conical surface of the roller-carrier. Each roller is composed of a roller cup in the shape of a frustum with a cylindrical hole that carries a bearing.

The size of the bearings used for the rollers (especially the inner rollers) is dictated by the smallest outside diameter found in catalogues for non-miniature parts. The radii of the conjugate cams, and consequently the size of the other components of the joystick and, thus, the size of the entire assembly, are decided upon based on the size of readily available standard bearings. The corresponding smaller cam diameter is calculated and specified as 100 mm, the bigger cam diameter as 136 mm. The roller-carrier is designed as a frustum shell open at the circle with bigger diameter. The surface of the roller-carrier is designed in such a way that once the roller stands are press-fitted in the holes on this surface, the stands are at an angle α_3. The value for α_3 is determined to be 48.13°, obtained using Eq. (9).

The spherical nature of the driving cams makes a gimbal frame suitable for mounting the cams coaxially as widely used in joystick design; one such example is the two-d.o.f joystick developed by Li et al. [13]. The diametrically opposed two-cam pairs are keyed to separate shafts; these cam-shafts are coaxially mounted on a shaft-carrier, the central element of the joystick, which carries all the shafts and ensures their proper orientation w.r.t. each other and, thus the proper engagement of the rollers on the roller-carrier with the cam lobes. The cam-shafts are mounted on one side on the gimbal frame with the help of ball bearings; on the other end they are keyed to the shaft-carrier. The roller-carrier is mounted on a shaft that is keyed to the shaft-carrier so that its axis is normal to that of the cam-shafts.The shaft-carrier has a counter-weight attached to it with the help of a threaded shaft in a diametrically opposite position w.r.t. the roller-carrier.

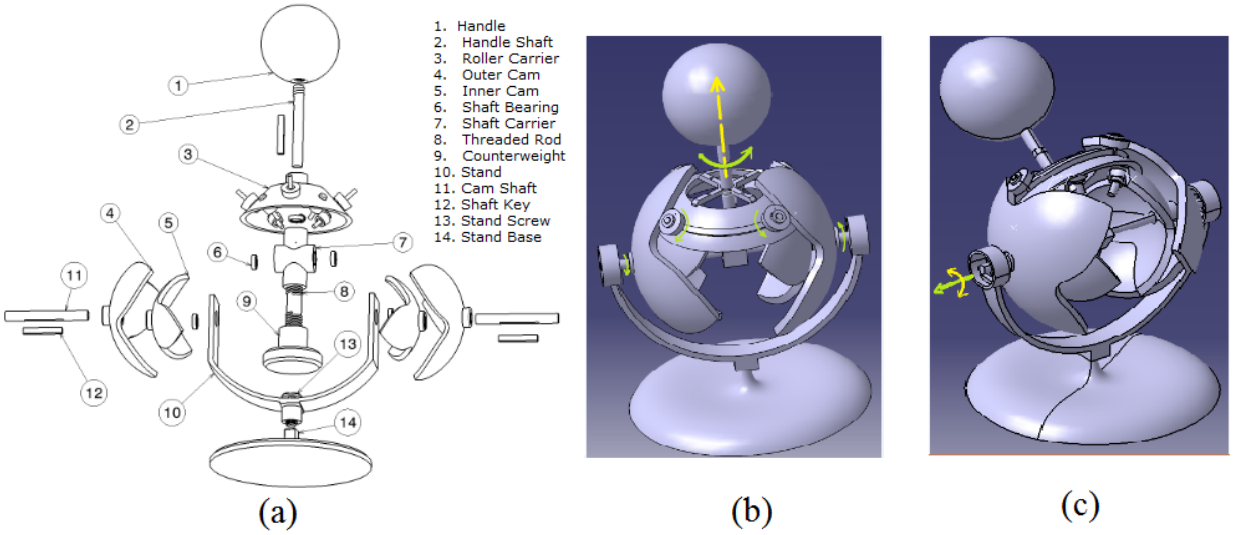

Fig. 7. (a) Exploded view of the joystick assembly; (b) Illustration of the roll motion; (c) Illustration of pitching motion of the joystick.

The shaft onto which the roller-carrier is keyed carries a spherical handle of a size suitable for a proper grip by an adult human hand. The gimbal frame carrying the shaft carrier with the mounted cams and roller-carrier is bolted to a disk-shaped stand for stable operation of the joystick. The overall height of the joystick assembly is smaller than 300 mm.The two larger cams are 98 mm in diameter. The exploded view of the joystick assembly is displayed in Fig. 7(a), the various parts comprising the mechanism being enumerated in the same figure.

6.2. Kinematics of the Pitch-Roll Joystick

The spherical cam mechanism implemented in the pitch-roll joystick functions, in principle, under negative action. The handle is attached to the roller-carrier. When torque is applied by the user on the handle, the roller-carrier drives the two sets of conjugate cams. On the other hand, when the motors respond with a torque emulating the elastic response of torsional springs, as required by haptics applications, the mechanism functions under positive action.

6.2.1. Rolling

The rolling of the joystick takes place about the roller-carrier axis. The two sets of cams rotate in opposite directions. One of the configurations of the joystick, while performing pitching motion, is depicted in Fig. 7(b).

At any time, there are three contact lines between one set of coaxial conjugate cams and their corresponding rollers. For the whole mechanism, there are a total of six contact lines. In one half of the rotation cycle of the roller-carrier, the outer cams have two contact lines, each with its neighboring outer rollers; for the inner cams, each has one contact line with the inner rollers. In the other half, the inner cams have two contact lines each, whereas the outer cams have just one contact line each. The reason why there is a different number of contact lines is that the inner and outer cams lie at a 60° phase angle.

6.2.2. Pitching

The pitching of the joystick takes place about the cam axis. In this case, the motion between the rollers of the roller-carrier and the corresponding cams becomes locked. The two pairs of conjugate cams then move

in the same direction. The contact lines do not change during this motion; they thus remain the same as if they were in the initial configuration at the point of initiation of pitching. One of the configurations of the joystick while performing pitching motion is depicted in Fig. 7(c).

7. CONCLUSIONS

The spherical cam mechanism provides a sound alternative to bevel gears for developing a pitch-roll joystick that targets haptics applications. The advantages of lower backlash, lower friction and higher stiffness, essential requirement for haptic devices, can compensate for the higher cost of manufacturing incurred in the case of cam mechanisms. These advantages are guaranteed by a continuous roller-cam contact and a pure-rolling motion between roller and cam when driving the joystick handle. The size of the joystick is dictated by both ergonomic studies on hand-driven joystick devices and the availability of small standard bearings. For a joystick of this size, the feasibility of machining the small components of the joystick assembly becomes an issue. Such a joystick is envisioned to be implemented as a haptic device. Future work should include augmenting the joystick with a force feedback system. The torque sensors are to be placed along the axis of the roller-carrier handle. Another task is developing haptics algorithms for such a joystick. Apart from employing the joystick as a haptic device, the joystick can also be used as a control device for manipulators, for example, for pick-and-place robots used in the packaging industry.

ACKNOWLEDGEMENTS

The authors acknowledge the support received from Canada's *Natural Sciences and Engineering Research Council* and Quebec's *Fonds de recherche Nature et Technologies*. The second author also acknowledges the support received from McGill University via a James McGill Professorship in Mechanical Engineering.

REFERENCES

1. Bai, S. and Angeles, J., "The design of spherical multilobe-cam mechanisms", *Journal of Mechanical Engineering Science*, Vol. 223, No. 3, pp. 473–482, 2009.
2. Wei, E.J., Lai, H.Y. and Chen C.K., "Machine tool setting for the manufacturing of spherical cams", *Journal of Material Processing Technology*, Vol. 100, pp. 147–155, 2000.
3. Karwowski, W., *International Encyclopedia of Ergonomics and Human Factors*, Taylor & Francis, London, UK, 2001.
4. Agronin, M.L., "The design of a nine-string six-degree-of-freedom force-feedback joystick for telemanipulation", in *Proceedings of the Workshop on Space Telerobotics*, Vol. 2, pp. 341–348, Pasadena, CA, USA, July 1, 1987.
5. Hayusmans, M.A., de Looze, M.P., Hoozemans, M.J.M., van der Beek, A.J. and van Dieën, J.H., "The effect of joystick handle size and gain at two levels of required precision on performance and physical load on crane operators", *Ergonomics*, Vol. 49, No. 11, pp. 1021–1035, 2007.
6. Takemoto, A., Yano, K., Miyoshi, T. and Terashima, K., "Operation assist control system of rotary crane using proposed haptic joystick as man-machine interface", in *Proceedings of the 2004 International Workshop on Robot and Human Interactive Communication*, pp. 533–538, Kurashiki, Okayama, Japan, September 20–22, 2004.
7. Beggs, J.S., *Advanced Mechanism*, The McMillan Company, New York, 1966.
8. McCarthy, J.M. and Roth, B., "Instantaneous properties of trajectories generated by planar, spherical, and spatial rigid body motions", *ASME Journal of Mechancial Design*, Vol. 104, No. 1, pp. 39–51, 1982.
9. González-Palacios, M.A. and Angeles, J., *Cam Synthesis*, Kluwer Academic Publishers, 1993.
10. Norton, R.L., *Design of Machinery. An Introduction to the Synthesis and Analysis of Mechanisms and Machines*, Second Edition, McGraw Hill, New York, 2001.

11. Nutbourne, A.W. and Martin, R.R., *Differential Geometry Applied to Curve and Surface Design, Vol. 1: Foundations*, Ellis Horwood Ltd., West Sussex, 1988.
12. Rutter J.W., *Geometry of Curves*, CRC Press LLC, Boca Raton, FL, 2000.
13. Li, W.H., Liu, B., Kosasih, P.B. and Zhang, X.Z., "A 2-DOF MR actuator joystick for virtual reality applications", *Sensors and Actuators A: Physical*, Vol. 137, No. 2, pp. 308–320, 2004.